# Hierarchical Nanotubes Constructed by CoSe$_2$ Nanorods with Oxygen-rich Surface for Efficient Oxygen Evolution Reaction

Baoming Jia,[a][†] Ziqian Xue,[a][†] Qian Liu,[a] Qinglin Liu,[a] Kang Liu,[b] Min Liu,[b] Ting-Shan Chan,[c] Yinle Li,[a] Zhijun Li,[d] Cheng-Yong Su,[a] Guangqin Li[a]*

a.    MOE Laboratory of Bioinorganic and Synthetic Chemistry, Lehn Institute of Functional Materials, School of Chemistry, Sun Yat-Sen University. Guangzhou 510275, P. R. China, E-mail: liguangqin@mail.sysu.edu.cn

b.    State Key Laboratory of Powder Metallurgy; Institute of Super-microstructure and Ultrafast Process in Advanced Materials, School of Physics and Electronics, Central South University, 932 South Lushan Road, Changsha, Hunan 410083, P. R. China.

c.    the synchrotron measurement at Taiwan Light Source (01C), Taiwan, China.

d.    Northeast Petroleum University, Daqing, 163318, P. R. China

† Both authors contributed equally to this manuscript.

## Experimental Section

### 1.1 Synthesis of Se NWs

The Se nanowires were first synthesized according to the Literature. [1] For the synthesis of Se NWs, analytically pure Na$_2$SeO$_3$ (2 mmol) and 5 mL of PVA (5 wt %) solution were added into 40 mL distilled water at room temperature to form a clear solution, which was then stirred strongly for about 30min and transferred into a 50 mL Teflon-lined stainless-steel autoclave. The autoclave was sealed and heated at 140 °C for 48 h before air-cooled down to room temperature. The turbid solution was collected and washed with distilled water and absolute alcohol for several times. The precipitate of the bottle was discarded. The red-brown powders were collected after drying in a vacuum at 60 °C for 12 h.

### 1.2 Synthesis of Se NWs@PPy

In a typical synthesis[2], 58 mL of 1.10 mg mL$^{-1}$ Se NWs aqueous solution and 0.2 mL of pyrrole were mixed, sonicated for 40 min, and stirred for 15 min. Subsequently, 50 mL of the 313.5 mg FeCl$_3$ · 6H$_2$O aqueous solution was added to the above mixed solution drop wisely under strong stirring. The system was agitated for 4 h for polymerization. The precipitate was collected after filtration and washed with ethanol and water.

### 1.3 Synthesis of Se NWs@PPy@ZIF-67

Se NWs@PPy aqueous solution (100 mL, 1mg • mL$^{-1}$) and 700 mg PVP(K30) were mixed and stirred for 4 h. The precipitate was separated by filtration and redispersed into 30 ml methanol solution containing 0.130 g of $Co(NO_3)_2 \cdot 6H_2O$. After constant stirring for 5 h, 1 mL 2-methylimidazole solution (300 mg • mL$^{-1}$) was poured quickly into the above mixed solution, followed by vigorous stirring for 2 h and aged for 24 h. Se Nws@ZIF-67 was prepared according to similar methods. 378 mg $Co(NO_3)_2 \cdot 6H_2O$ was dispersed in 30 mL Se NWs methanol solution (2.63 mg mL$^{-1}$). Then, 2.8 mL 2-methylimidazole solution (300 mg mL$^{-1}$) was poured quickly into above mixed solution.

**1.4 Synthesis of O-CoSe$_2$-HNT**

50 mg Se NWs@PPy@ZIF-67 was placed in a tube furnace and calcined at 300℃ for 2h with a ramp rate of 5℃ min$^{-1}$ in Ar atmosphere.

**1.5 Synthesis of CoSe$_2$-S**

100 mg ZIF-67 was placed in a tube furnace, and 0.5 g of Se powder was placed at the upstream side. This was followed by calcination at 300℃ for 2 h with a ramp rate of 5℃ min$^{-1}$ in Ar atmosphere.

**2. Characterizations:**

The morphology and structure of the samples were characterized by field-emission scanning electron microscopy (FESEM; Hitachi SU8010, 5 kV), transmission electron microscopy (TEM; JEOL, JEM-1400, 120 kV), and spherical aberration correction electron microscope (JEOL, ARM200, 300kV). Powder X-ray diffraction (XRD) patterns were recorded on a MiniFlex 600 (Rigaku Co., Japan) diffractometer with Cu Kα (λ = 1.5418 A) radiation. The N$_2$ adsorption-desorption isotherms were collected using a Micromeritics Instruments 3Flex at 77 K. The surface properties of the products were analyzed with X-ray photoelectron spectroscopy (XPS; VG ESCALABMKII instrument) with a Mg Kα X-ray source. X-ray adsorption near edge structure (XANES) and extended X-ray absorption fine structure (EXAFS) were collected by employing synchrotron radiation light source at 01C1 beam line of the National Synchrotron Radiation Research Center, Taiwan. The measurements were conducted in the Transmission mode. The data were processed with IFEFFIT.[3] Fourier transformation was k3-weighted in the k range from 3 to 12 Å$^{-1}$.

**Electrochemical measurements**

All the electrochemical measurements were implemented on a CHI 760E electrochemical workstation (CH Instruments, Inc., Shanghai) through a standard three-electrode system. A glassy carbon electrode (3 mm in diameter) was used as the working electrode. 5 mg of the catalysts and 20 μL Nafion solution were dispersed in 490 μL ethanol and 490 μL water, which was sonicated for 45 min to form ink. Then, 5μL of the mixture ink was dripped onto the surface of glassy carbon electrode and dried at room temperature. The Ag/AgCl electrode and platinum wire were used as the reference electrode and counter electrode, respectively. The OER performance was evaluated in 1 M KOH solution. The samples were evaluated by obtaining the polarization curves via linear sweep voltammetry (LSV) at a scan rate of 10mV·s$^{-1}$. Electrochemical impedance spectroscopy (EIS) measurements were carried out at different potentials from 105 to 0.01 Hz. The stability tests were performed by cyclic voltammetry (CV) scanning for 2000 cycles (CV, 100 mV · s$^{-1}$) for OER and long-term chronoamperometry. CV tests were also used to define the electrochemical double-layer capacitances ($C_{dl}$). The electrochemically active surface area could be assessed from the plot slope of the charging current vs. the scan rate. All the polarization curves in this work were carried out with iR compensation. Turnover frequency (TOF) calculation of the catalysts: The TOF value was calculated from the equation

$$TOF = \frac{J \, x \, A}{4 \, x \, F \, x \, m}$$

where J is the current density at a given overpotential ( $\eta$ = 300 mV), A is the surface area of the electrode, F is the Faraday constant (96485 C · mol$^{-1}$), and m is the number of moles of metal on the electrode. All the Co atoms were assumed to be accessible for catalysing the OER.

**RHE calibration**

The potential was calibrated with respect to reversible hydrogen electrode (RHE) according to previous report.[4] The calibration was performed in the high purity hydrogen saturated electrolyte with a Pt foil as the working electrode. CVs were run at a scan rate of 1 mv s$^{-1}$, and the average of the two potentials at which the current crossed zero was taken to be the thermodynamic potential for the hydrogen electrode reactions.
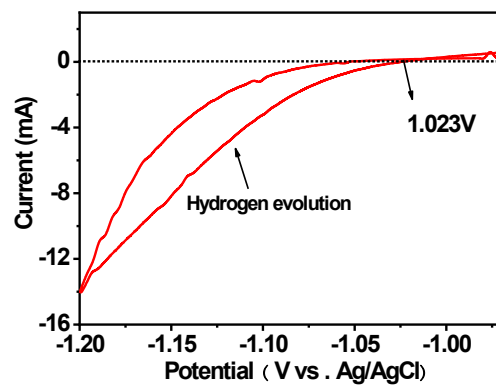
So, in 1 M KOH, $E_{RHE} = E_{Ag/AgCl} + 1.023$

# 3. Results and discussion
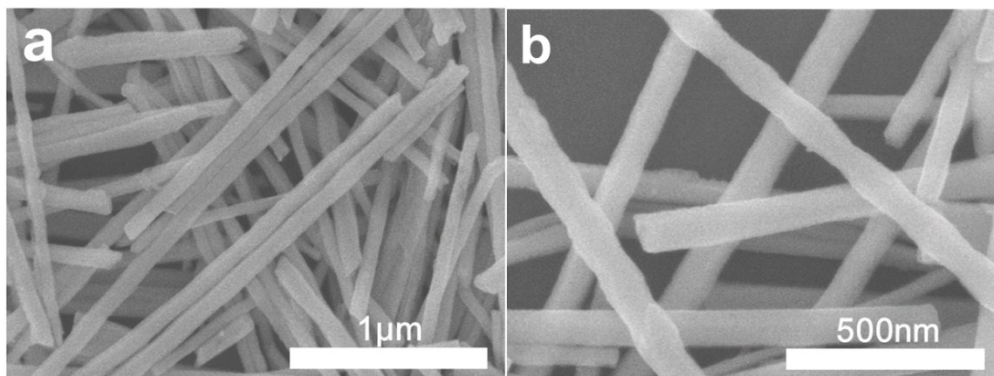


**Figure S1.** SEM images of Se NWs.
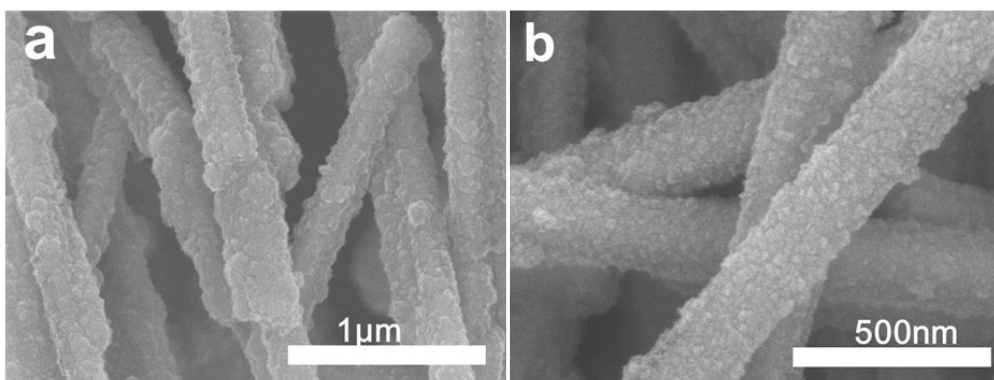


**Figure S2.** SEM images of the as-synthesized Se NWs@PPy.
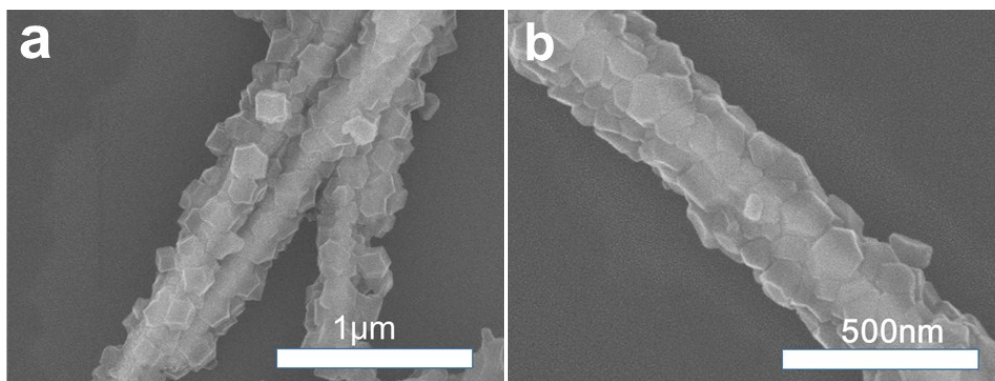
**Figure S3.** SEM images of the as-synthesized Se NWs@PPy@ZIF-67.
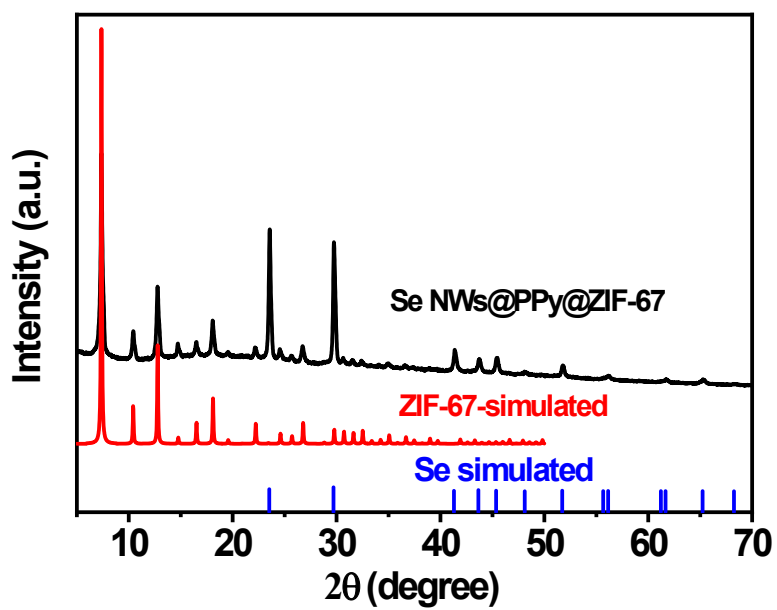


**Figure S4.** XRD patterns of Se NWs@PPy@ZIF-67.
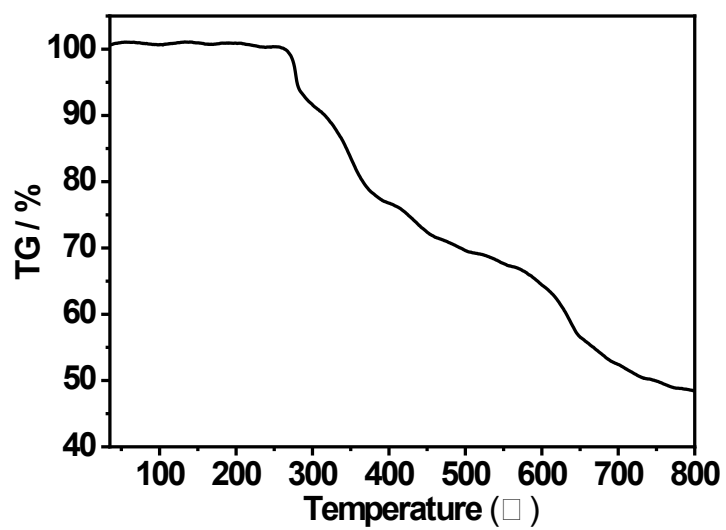
**Figure S5.** TGA curve of the as-synthesized Se NWs@PPy@ZIF-67.
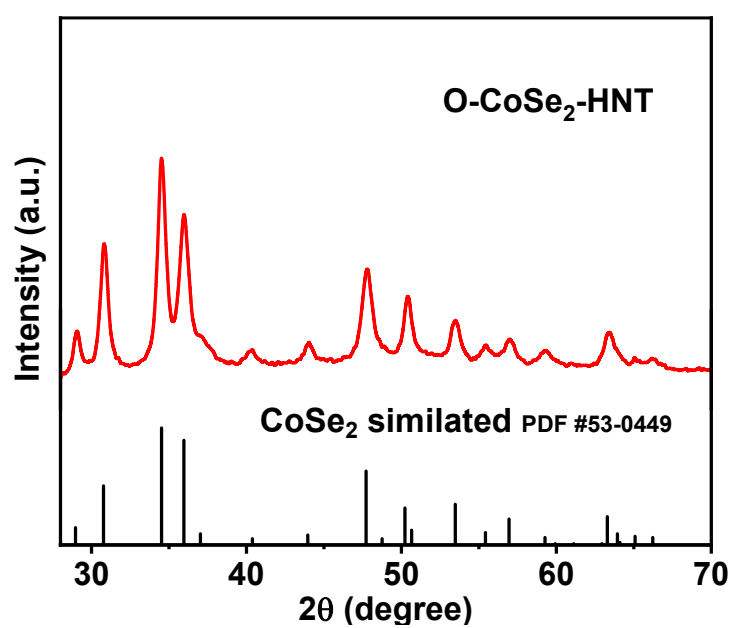


**Figure S6.** XRD of the as-prepared O-CoSe$_2$-NHT.
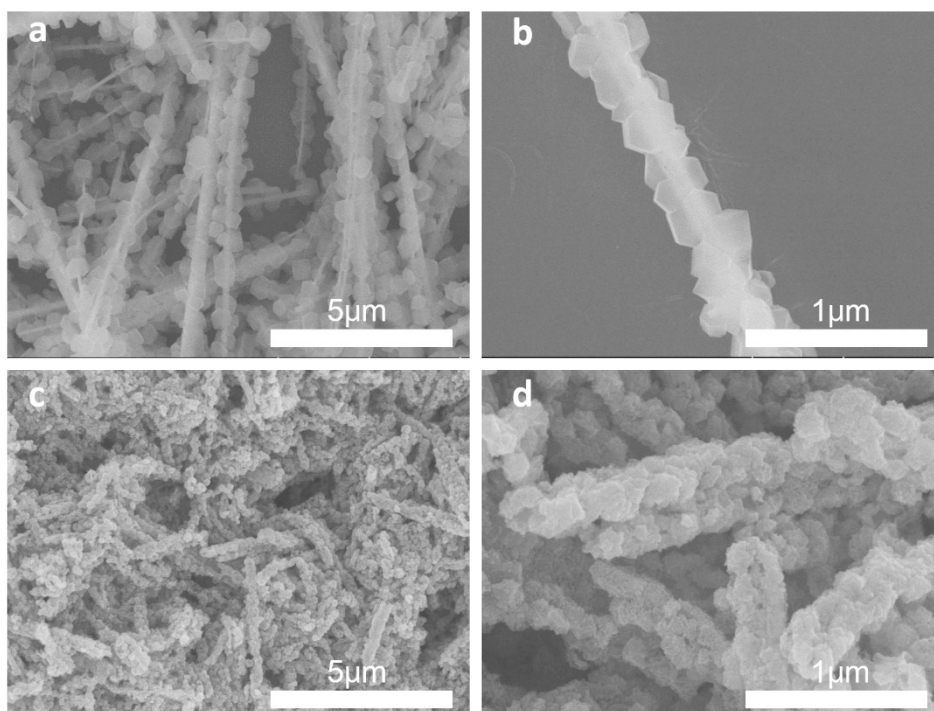
**Figure S7.** a,b) SEM images of the as-synthesized Se NWs@ZIF-67(without PPY). c,d) SEM images of the corresponding pyrolysis product.
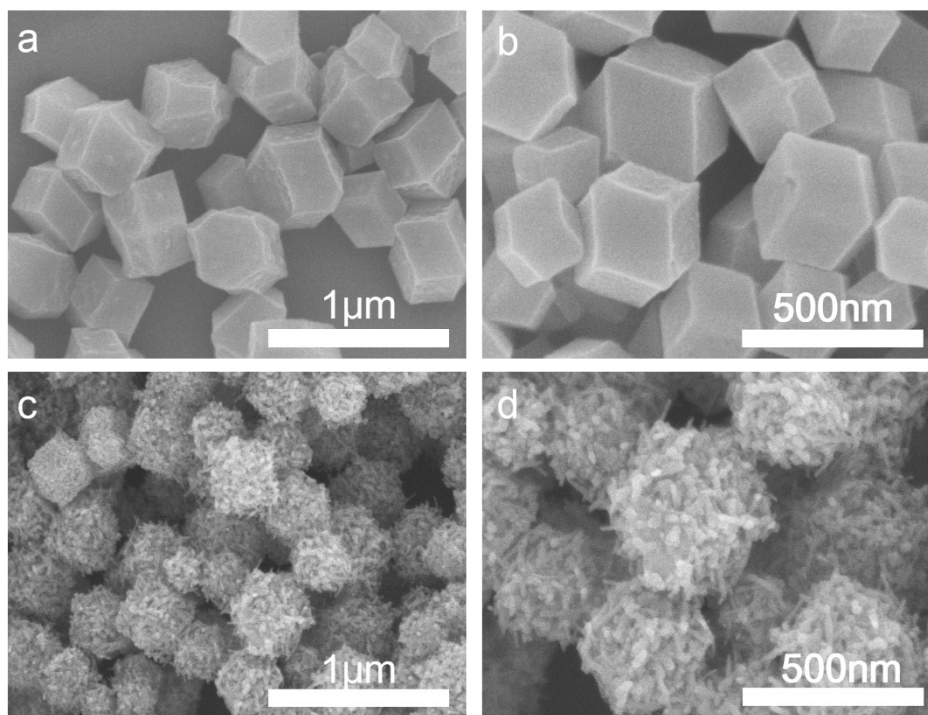


**Figure S8.** a) and b) SEM images of the as-synthesized ZIF-67. c) and d) SEM images of the corresponding pyrolysis product.
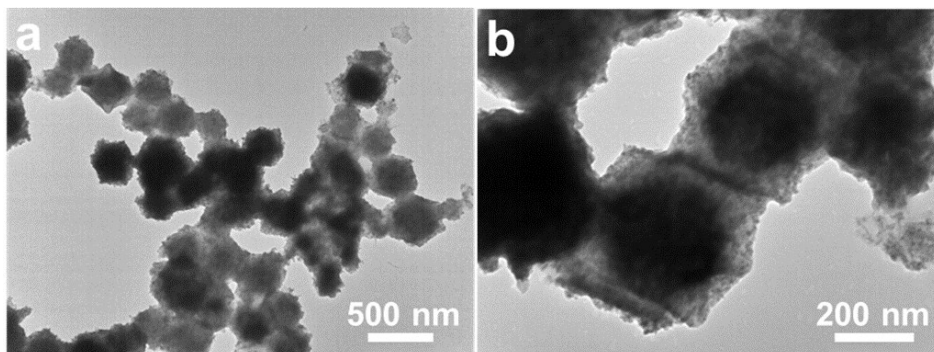
**Figure S9.** TEM images of the as-synthesized CoSe$_2$-S.
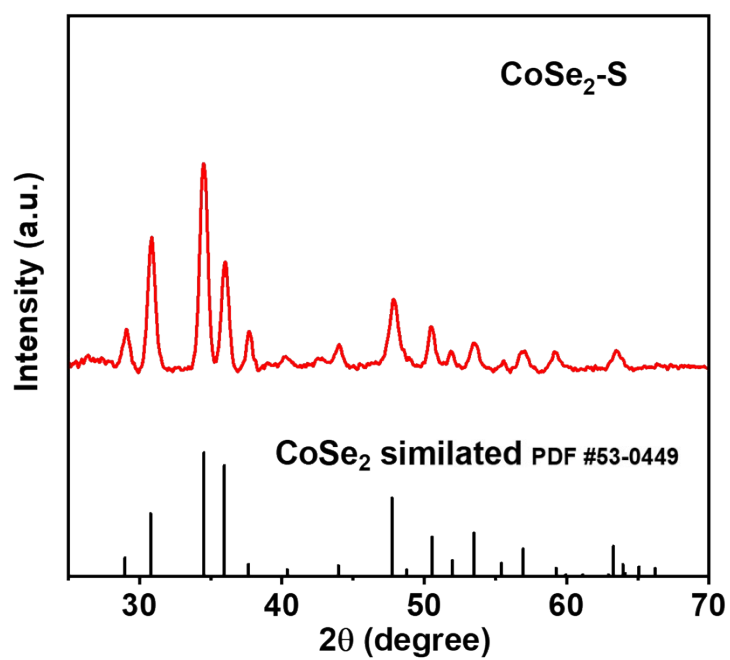


**Figure S10.** XRD of CoSe$_2$-S prepared by calcining ZIF-67 and Se powder.
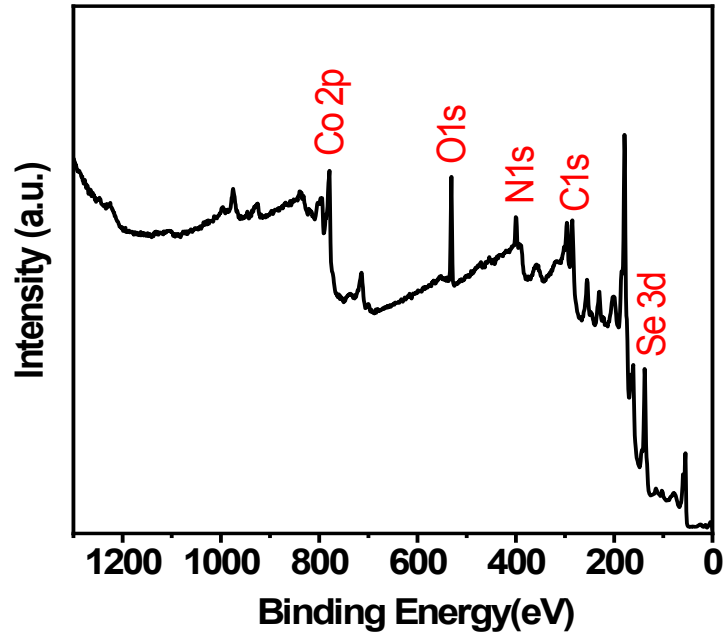
**Figure S11.** XPS survey spectrum of CoSe$_2$-S.
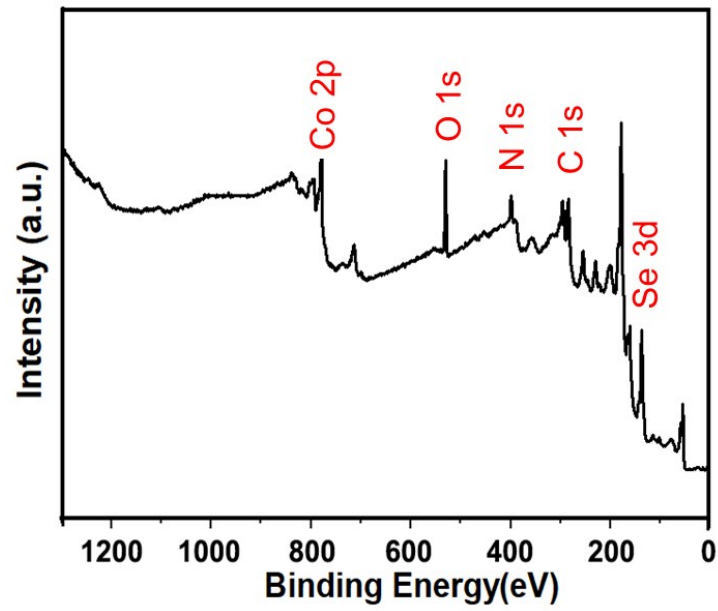


**Figure S12.** XPS survey spectrum of mace-like O-CoSe$_2$-HNT.
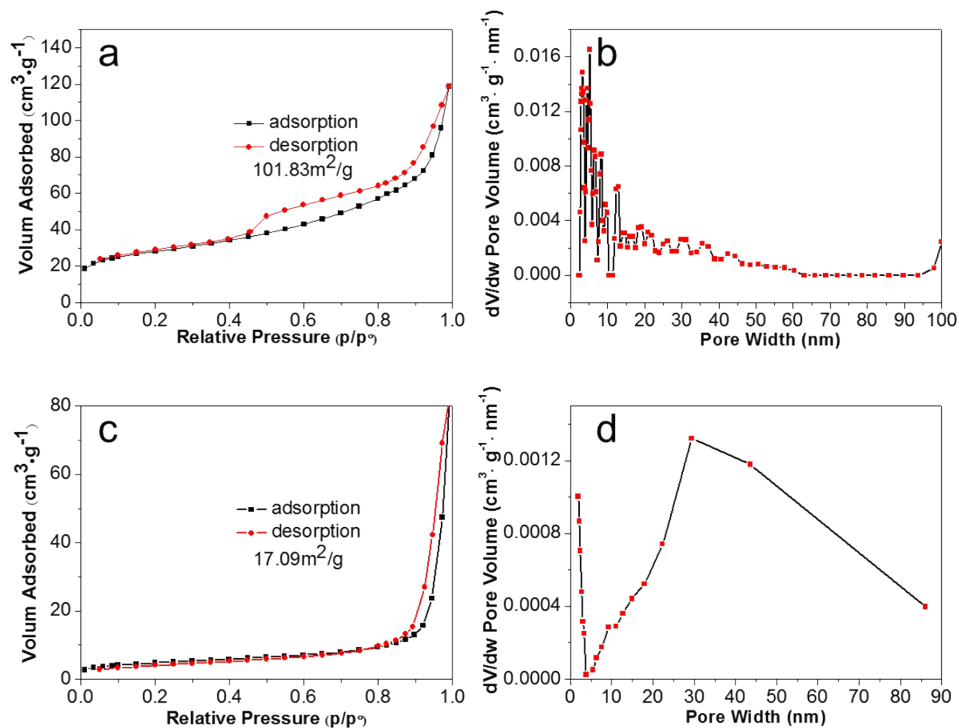
**Figure S13.** a) and b) $N_2$ adsorption-desorption isotherm and size distribution curves of mace-like O-CoSe$_2$-HNT. c) and d) $N_2$ adsorption-desorption isotherm and size distribution curves of CoSe$_2$-S catalyst.
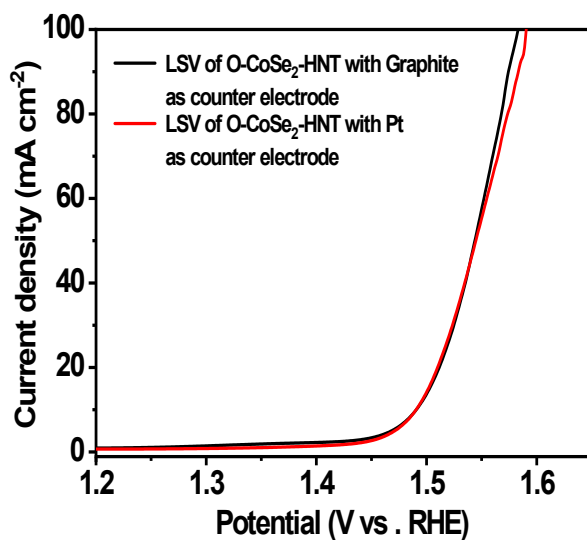


**Figure S14.** LSV curves of O-CoSe$_2$-HNT using different counter electrode.

**Table S1.** EIS results of different catalysts.

| Catalyst | O-CoSe$_2$-NHT | CoSe$_2$-S | IrO$_2$ | RuO$_2$ |
|---|---|---|---|---|
| R$_s$ (ohm) | 13.4 | 14.2 | 12 | 13 |
| R$_{ct}$ (ohm) | 37.9 | 90.4 | 50.9 | 44.5 |
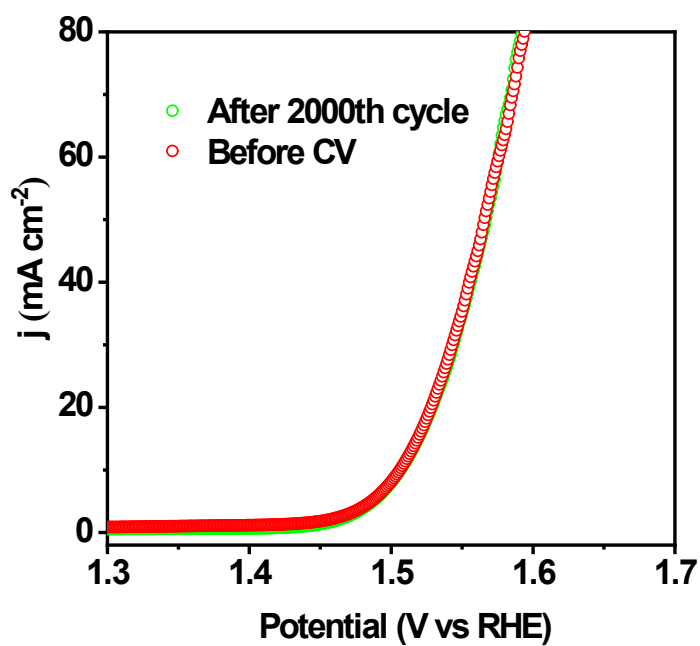


**Figure S15.** LSV curves of O-CoSe$_2$-HNT before and after 2000 CV cycles.
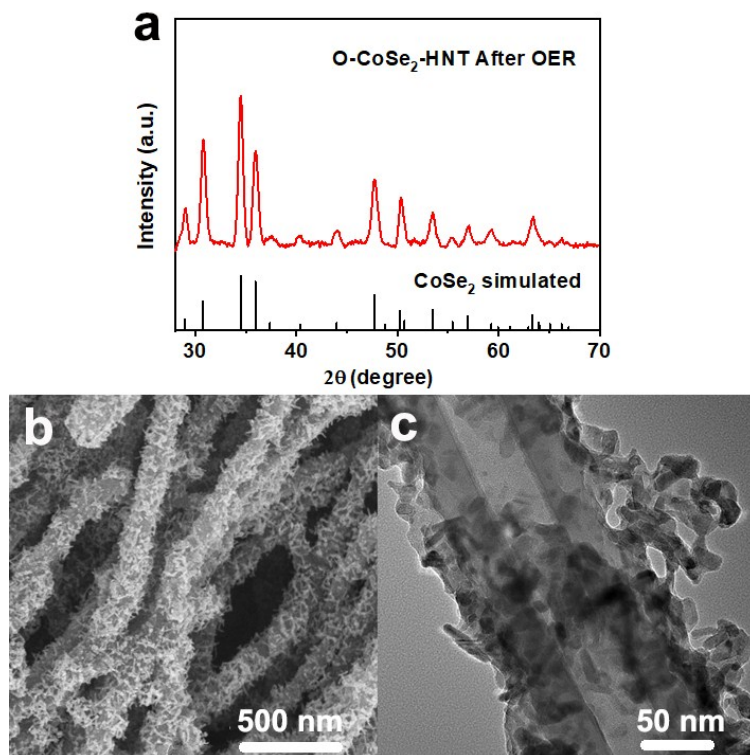
**Figure S16.** a) XRD pattern, b) SEM and c) TEM images of the of O-CoSe$_2$-HNT catalyst after long term test in 1 M KOH for OER.
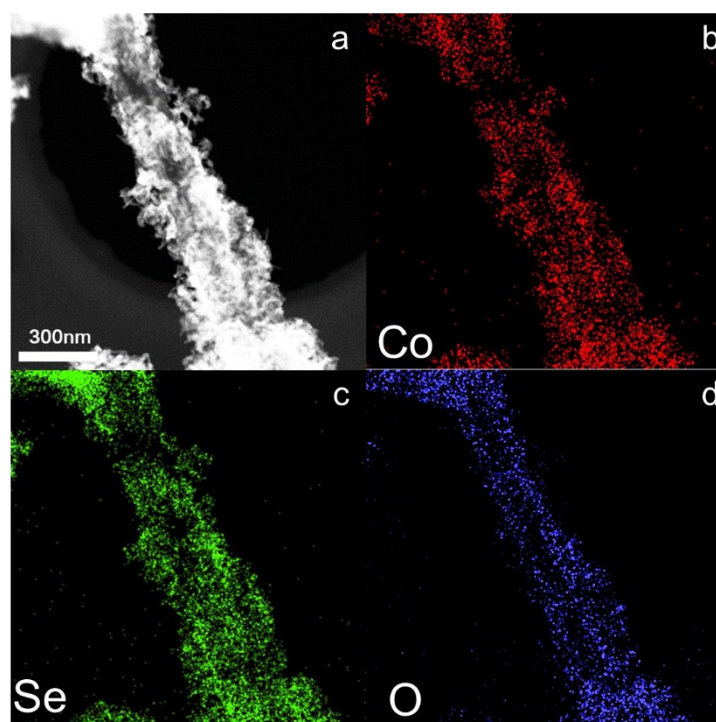
**Figure S17.** a-d) HAADF-STEM elemental mapping spectra of O-CoSe$_2$-HNT catalyst after long term test in 1 M KOH for OER.
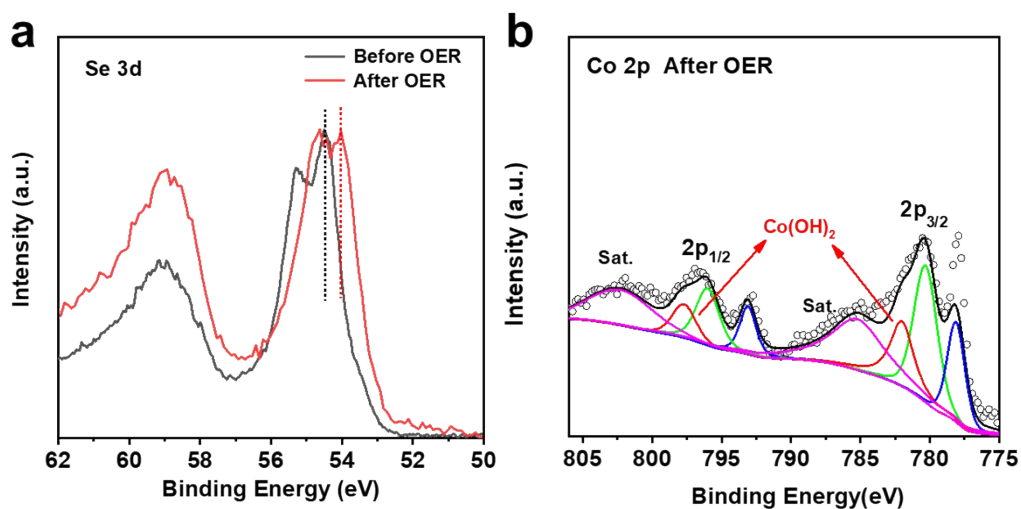


**Figure S18.** a) Se 3d and b) Co 2p of O-CoSe$_2$-HNT after long term test in 1 M KOH for OER.
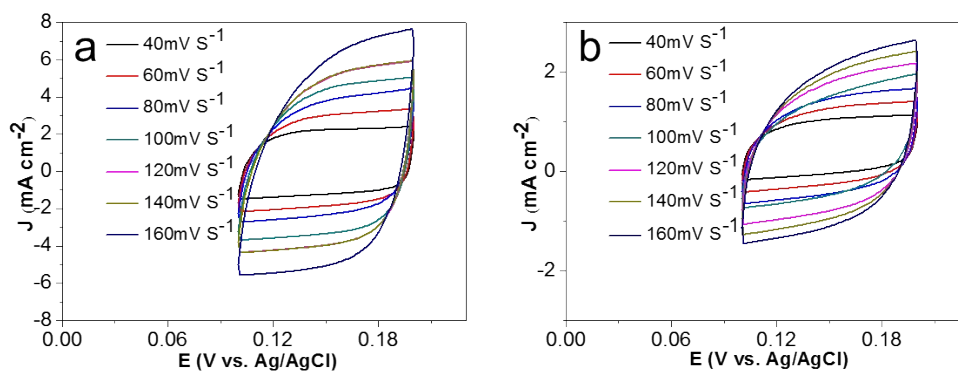


**Figure S19.** CV of a) O-CoSe$_2$-HNT and b) CoSe$_2$-S in 1 M KOH solution in the region of 0.1-0.2 V vs. Ag/AgCl.
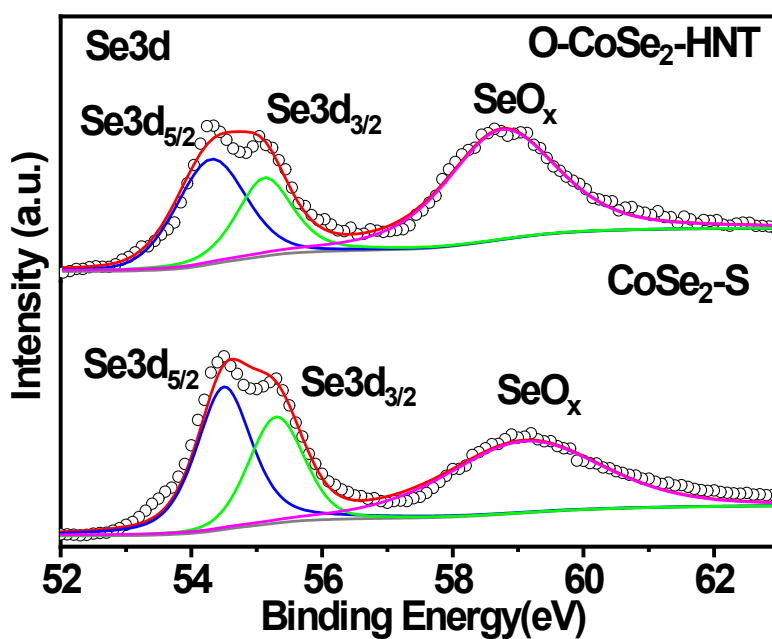
**Figure S20.** Se 3d of O-CoSe$_2$-HNT and CoSe$_2$-S.
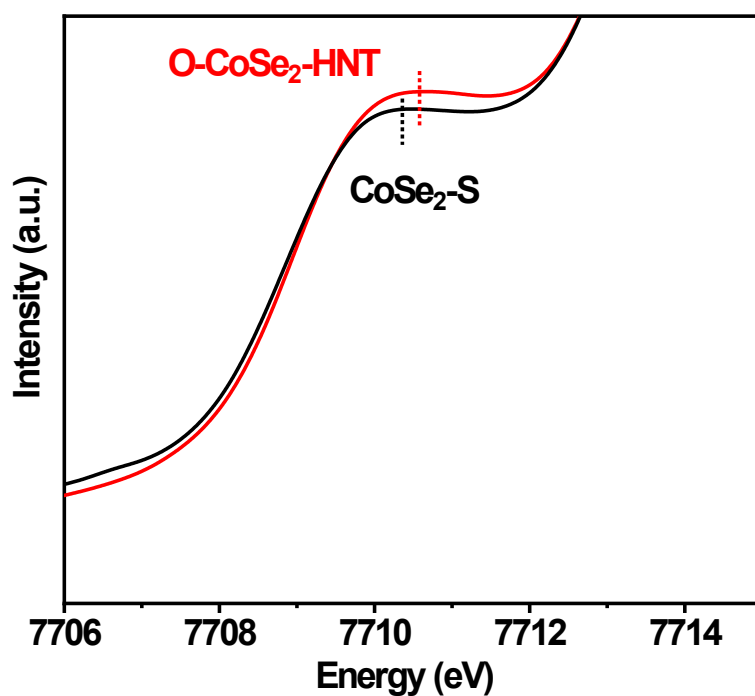


**Figure S21.** XANES pre-edge peaks of O-CoSe$_2$-HNT and CoSe$_2$-S.

15
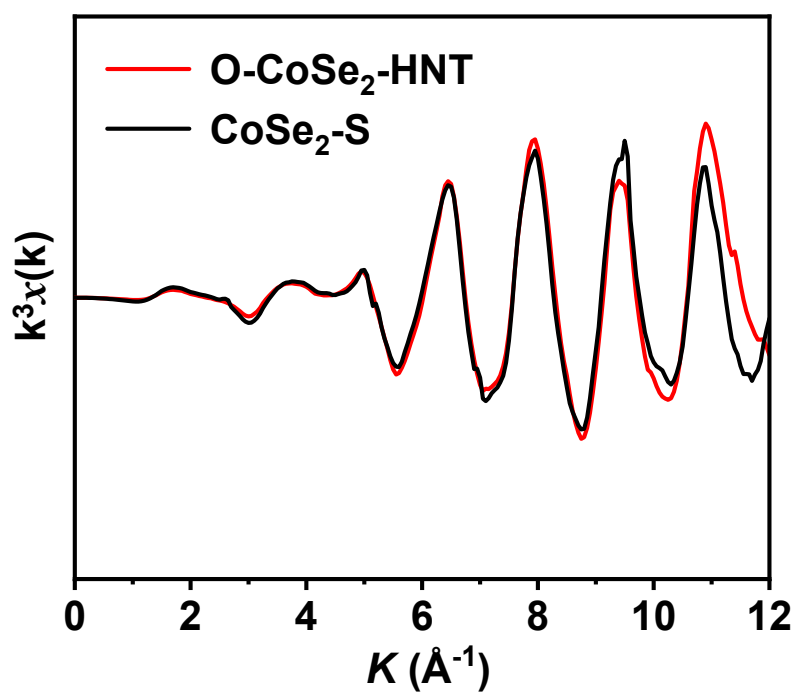
**Figure S22.** The Co K-edge extended XAFS oscilation function.
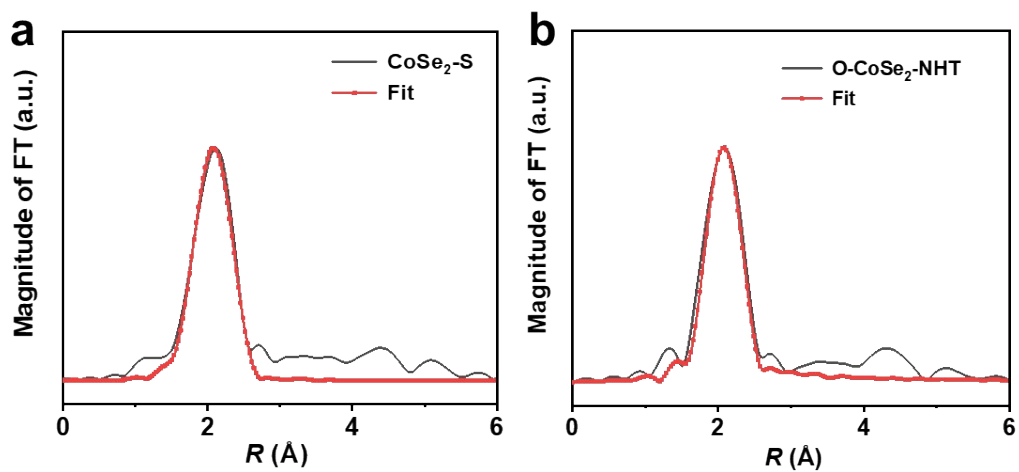


**Figure S23.** The EXAFS fitting results of the Co edge for CoSe$_2$-S and O-CoSe$_2$-HNT.

**Table S2.** Summary of various Co-based non-noble metal catalysts for OER in 1 M KOH.

| Catalyst | Overpotential at 10 mA · cm$^{-2}$ | Tafel slope (mV · dec$^{-1}$) | Reference |
|---|---|---|---|
| **O-CoSe$_2$-HNT** | **252** | **62** | **This work** |
| Co-P films | 345 | 47 | *Angew. Chem. Int.Ed*. **2015**, *127*, 6349 |
| CoO$_x$@CN | 385 | N/A | *J. Am. Chem. Soc*. **2015**, *137*, 2688 |
| Au$_{25}$/CoSe$_2$ | 430 | NA | *J. Am. Chem. Soc*. **2017**, *139*, 1077 |
| CoSe$_2$ nanoparticles | 297 | 41 | *Nano Res*. **2016**, *9*, 2234 |
| CoMnP | 330 | 61 | *J. Am. Chem. Soc*. **2016**, *138*, 4006 |
| ultrathin N-CoFe LDHs | 281 | 40.03 | *Adv. Funct. Mater*. **2018**, *28*, 1703363 |
| P-Co$_3$O$_4$ | 280 | 51.6 | *Energy Environ. Sci*., **2017**, *10*, 2563 |
| CoSe$_{2-x}$-Pt | 255 | 31 | *Adv. Mater*. **2018**, *31*, 1805581 |
| (Co/Fe)$_4$O$_4$ | 300 | 36 | *ACS Catal*. **2019**，DOI: 10.1021/acscatal.9b00293 |
| Co$_3$O$_4$-HPNSs | 308 | 60.78 | *J. Mater. Chem. A*, **2019**, DOI: 10.1039/C9TA00330D |
| CoOOH hollow nanospheres | 275 | 49 | *J. Mater. Chem. A*, **2019**, *7*, 7777 |
| NCoM-Cb-Ar | 340 | 76 | *Angew. Chem. Int. Ed*. **2019**，DIO: |

| | | | |
|---|---|---|---|
| $(Co_{0.21}Ni_{0.25}Cu_{0.54})_3Se_2$ | 272 | 53.3 | *J. Mater. Chem. A*, **2019**, DOI: 10.1039/C9TA00863B |
| $Co_2(OH)_3Cl$ | 270 | 155 | *Adv. Mater*. **2019**, *31*, 1805127 |
| CoOOH-NS | 253 | - | *Energy Environ. Sci.,* **2019***, 12, 739* |

**Table S3.** EXAFS fitting results of the Co edge for $CoSe_2$-S and O-$CoSe_2$-HNT.

| Sample | Shell | N | R (Å) | $\sigma^2 (x10^{-3}\,Å)$ | $\triangle E_0$ (eV) |
|---|---|---|---|---|---|
| **$CoSe_2$-S** | Co-Se | 6±0.4 | 2.41±0.2 | 5.8 | -1.1 |
| **O-$CoSe_2$-HNT** | Co-Se | 5.3±0.4 | 2.39±0.2 | 6.6 | -1.1 |

N, coordination number; R, distance between centre and backscatter atom; $\sigma^2$, the Debye-Waller factor value; $\triangle E_0$, inner potential correction to account for the difference in inner potential between the sample and the reference.

**References**

1. S. Xiong, B. Xi, W. Wang, C. Wang, L. Fei, H. Zhou, and Y. Qian, *Cryst. Growth Des*., 2006, **6**, 1711-1716

2. Z. Y. Wu, X. X. Xu, B. C. Hu, H. W. Liang, Y. Lin, L. F. Chen and S. H. Yu, *Angew. Chem. Int. Ed*., 2015, **54**, 8179-8183.

3. B. Ravel, M. Newville, *J. Synchrotron Radiat.*, 2005, **12**, 537-541.

4. Y. Liang, Y. Li, H. Wang, J. Zhou, J. Wang, T. Regier, H. Dai, *Nat. mater*, 2011, **10**, 780-

786.